The 2010 IEEE/RSJ International Conference on
Intelligent Robots and Systems
October 18-22, 2010, Taipei, Taiwan

Design of a Linear Haptic Display Based on Approximate Straight Line Mechanisms

M. Joinié-Maurin, L. Barbé, O. Piccin, J. Gangloff and B. Bayle
LSIIT, UMR ULP-CNRS 7005
Pole API, Bd. S. Brant, 67412 Illkirch, France

R. Rump
INSA-Strasbourg
67084 Strasbourg, France

Abstract— **In this paper, we study a class of one degree-of-freedom mechanisms in order to design linear haptic interfaces. They allow to perform straight line motions with only revolute joints, thus limiting the friction that characterizes linear bearings. We particularly describe the characteristics of these systems and their good properties to design haptic displays: parallel architecture, very good linearity, good use of the actuator torque. The Hoeken's mechanism which has the best characteristics to build a direct drive general purpose haptic display is selected. We present the fabricated prototype and its evaluation in terms of bandwidth, Coulomb friction and apparent mass.**

I. Introduction

While haptics has become a very popular technology, there are only a few simple systems to introduce force feedback principles. The main family of such systems is the haptic paddle which was designed to illustrate the complete integration of an haptic device in the context of an undergraduate dynamic systems course [1], [2]. The haptic paddle is a one degree-of-freedom (DOF) device with a cable-pulley transmission and a basic control system using low cost components. The system has a very simple modeling, which is certainly an advantage from the pedagogical point of view. However, its manipulation along a circular path is not very intuitive.

In our opinion, programmed impedances could be rendered more naturally by moving along a straight path. To our knowledge, there are very few haptic interfaces with a simple linear mobility. Rather, most haptic interfaces use decoupled rotations, so that a straight line path is generally obtained by combining several DOF and using virtual fixtures that guide the motion along the straight line [3]. Though these techniques have already led to interesting results, it is natural to believe that they are however less effective than dedicated mechanical systems.

There are two solutions to achieve a straight motion with force feedback:

- the first one is to use a linear actuator [4], [5]. These motors exhibit high forces with respect to their volume and can then be used as direct drive actuators. However, they have some drawbacks with respect to haptic applications. As they are very similar to brushless rotary motors, they suffer from magnetic cogging which involves undesirable force ripple. Also, the motor translation is limited with respect to the motor length, specially for small size linear motors. Finally, the slider is heavy which is a limitation for transparent haptic rendering;
- the second and by far the most usual choice to design a prismatic active joint is to use a rotary motor combined with a motion transformation mechanism including a linear guidance system. It generally involves either an important number of joints or systems with gears. In the case of a haptic device, the design of such a mechanism has to be compatible with demanding specifications: limited friction, low inertia, compactness and of course low price, if possible [6].

The 3-DOF linear haptic display Excalibur [7] has long been the only linear haptic display. It is characterized by a large workspace and large output forces: 300 mm range of motion for the x and $y-$axis, 200 mm for the $z-$axis; 200 N peak forces and 100 N continuous forces. It is particularly well adapted to applications for which a good structural stiffness is required. At the contrary, its use is limited with regard to fine manipulations, most notably because of Coulomb friction. Therefore, it does not correspond to a general purpose or an educational device.

More recently, Weir et al. [8] presented a linear system dedicated to high performance force rendering, with a low apparent mass of 5 grams and a very fine sensing resolution of 0.5 μm, in order to simulate a linear switch. It is based on a 4-bar mechanism, with a small range of motion of 15 mm, in order to approximate a linear motion. Though not particularly developed by the authors in [8], the choice of a 4-bar system is specially relevant to approximate linear motions with revolute joints. In the following, we will apply this property of the 4-bar linkage to design a compact, direct drive, linear haptic device, with general purpose characteristics, combining a reasonable range of motion of 50 mm with an output force of 5 N. The goal of this device is for educational support and for teleoperation testbed (medical environment simulation).

The paper is organized as follows. In section II, we introduce the approximation of rectilinear motions using 4-bar mechanisms. We compare different solutions through a small number of characteristics that are significant in terms of haptics. The Hoeken's mechanism is selected after its good properties have been emphasized. In section III, we present the resulting prototype and illustrate its performances: bandwidth, apparent mass, Coulomb friction and

stiffness capability. Conclusions and perspectives are finally given.

II. Straight line mechanisms

In the preliminary design stages, we selected possible architectures based on: i) a rack and pinion mechanism; ii) a ball screw mechanism; iii) a cable mechanism; iv) a slider-crank mechanism. When comparing the relative merits of these solutions, the first two mechanisms were found not adapted to haptic applications, not efficient enough in the first case, not backdrivable enough in the second one. We then focused on the two other solutions, to propose two alternative designs [9]. The first one is based on a cable transmission mechanism, which is the simplest and more intuitive architecture. We then considered the slider-crank mechanism, whose use is quite original in this context to design a linear haptic device.

Whatever the considered transformation mechanism, it includes a prismatic pair with linear bearings, which are necessary to limit friction. However, they introduce much more friction than conventional ball bearings and have to be preloaded for optimal use. While the manufacturing of a prismatic pair with very limited friction is challenging, either exact or approximate straight lines can be obtained with mechanisms built from only revolute joints [10]. The systems providing exact straight motions as the Peaucellier's mechanism have an important number of joints (8 for Peaucellier's) and are not very compact. In return, approximate straight lines can be obtained with mechanisms based on the 4-bar linkage, with a few number of different solutions that depend on the choice for the bars lengths. In the following we present the most interesting solutions.

A. Possible solutions

A 4-link mechanism can be represented without loss of generality as shown in Fig. 1. Each link is positioned with

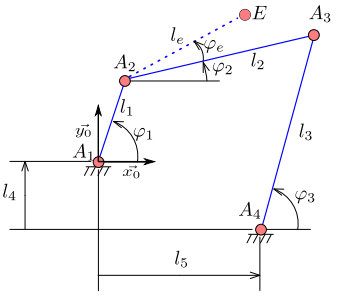

Fig. 1. Generic 4-link mechanism.

respect to the conventions of the figure. The reference frame $R_0 = (A_1, \overrightarrow{x_0}, \overrightarrow{y_0})$ is centered on the active joint. Let $\varphi_i = (\overrightarrow{x_0}, \overrightarrow{x_i})$, then the angle φ_1 is the input parameter. The end effector attached to the A_2A_3 coupler is defined by the parameters φ_e and l_e.

The 4-bar linkage modeling is a classical problem in mechanics, that we shortly recall to give a self contained description of the system. The loop closure equation of the 4-bar linkage writes: $\overrightarrow{A_1A_2} + \overrightarrow{A_2A_3} + \overrightarrow{A_3A_4} = \overrightarrow{A_1A_4}$. Making an orthogonal projection in R_0 results in the following system of equations:

$$l_1 \cos\varphi_1 + l_2 \cos\varphi_2 - l_3 \cos\varphi_3 = l_5 \quad (1)$$

$$l_1 \sin\varphi_1 + l_2 \sin\varphi_2 - l_3 \sin\varphi_3 = l_4 \quad (2)$$

Solving for the previous system gives:

$$\varphi_2 = 2 \arctan \frac{B \pm \sqrt{A^2 + B^2 - C^2}}{A + C} \quad (3)$$

where

$$A = 2 l_2 (l_1 \cos\varphi_1 - l_5) \quad (4)$$

$$B = 2 l_2 (l_1 \sin\varphi_1 - l_4) \quad (5)$$

$$C = {l_3}^2 - {l_1}^2 - {l_2}^2 - {l_4}^2 - {l_5}^2 + 2 l_1 (l_5 \cos\varphi_1 + l_4 \sin\varphi_1) \quad (6)$$

and

$$\cos\varphi_3 = \frac{l_1 \cos\varphi_1 + l_2 \cos\varphi_2 - l_5}{l_3} \quad (7)$$

$$\sin\varphi_3 = \frac{l_1 \sin\varphi_1 + l_2 \sin\varphi_2 - l_4}{l_3} \quad (8)$$

Then, the direct kinematic model can be obtained as:

$$x_e = l_1 \cos\varphi_1 + l_e \cos(\varphi_2 + \varphi_e) \quad (9)$$

$$y_e = l_1 \sin\varphi_1 + l_e \sin(\varphi_2 + \varphi_e) \quad (10)$$

The expressions of $\dot{\varphi}_2$ and $\dot{\varphi}_3$ in terms of $\dot{\varphi}_1$ can be calculated by differentiating equations (1) and (2) to obtain

$$\dot{\varphi}_2 = \frac{l_1 \sin(\varphi_3 - \varphi_1)}{l_2 \sin(\varphi_2 - \varphi_3)} \dot{\varphi}_1, \quad \dot{\varphi}_3 = \frac{l_1 \sin(\varphi_2 - \varphi_1)}{l_3 \sin(\varphi_2 - \varphi_3)} \dot{\varphi}_1 \quad (11)$$

By differentiating equations (9) and (10), the direct differential kinematic model can be found. Finally, after substitution of $\dot{\varphi}_2$ from equation (11), the direct differential kinematic model can be rearranged and written as :

$$\dot{p} = J \dot{\varphi}_1 \quad (12)$$

where $p = (x_e \; y_e)^T$ and J denote the operational coordinates and the (2×1)-dimensional Jacobian matrix of the mechanism. Singularities are avoided by restricting workspace with end stops.

Depending on the geometric parameters of the system, a part of the end effector motion might find to be nearly linear. We believe that several such approximate straight line mechanisms comply with the expected specifications for a 1-DOF linear haptic display. So, we particularly studied the more compact ones, which are: the Hoeken's, the Roberts, and the two Chebychev straight line mechanisms [10]. The first Chebychev mechanism has crossed legs while the so-called V type mechanism is similar to the Hoeken's mechanism but uses other geometry and workspace [10].

All these systems are represented in Fig. 2 where the straight part of their end effector motion has been considered. The simulations correspond to properly chosen dimensions, so as to obtain the desired tool range of motion of 50 mm. The angular range $\Delta\varphi_1$ corresponds to the whole linear motion. Note that for all these mechanisms $l_4 = 0$. In the figure, the initial and final configuration of the mechanism

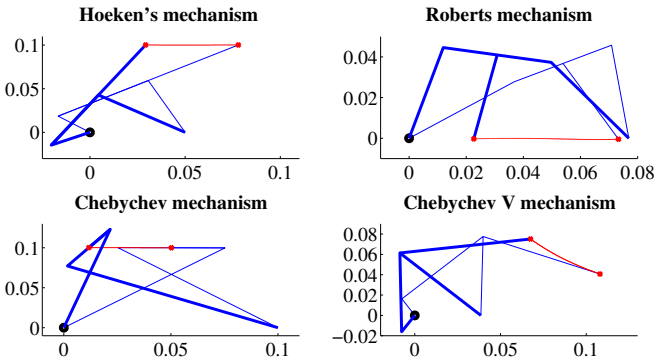

Mechanism	l_1/l_2	l_2	l_3/l_2	l_4/l_2	l_5/l_2
Hoeken	0.4	62.5 mm	1	0	0.8
Roberts	1.2	38.46 mm	1.2	0	2
Chebychev	2.5	50 mm	2.5	0	2
Chebychev V	0.23	77.5 mm	1	0	0.5

Mechanism	φ_e	l_e/l_2	φ_{1min}	φ_{1max}	$\Delta\varphi_1$
Hoeken	0	2	132	216	84
Roberts	-65.7	1.2	37	75	38
Chebychev	0	0.5	53	80	27
Chebychev V	-40.3	1.52	115	245	130

Fig. 2. The four mechanisms (angles in deg).

are represented, together with the trajectory of the end effector (remark: unit=meter in the figures).

B. Straight line mechanisms performances

For haptic applications, the goal is to provide a transparent straight line. The quality of the straight motion is fundamental: lateral motions must not be perceptible. Besides, another important criteria is the ability to build a compact direct drive system. So, the ratio (input torque/output force) and the dimensions were particularly examined. We evaluated the performances of systems whose dimensions were chosen to allow a 50 mm translation. For each mechanism, typical characteristics have been evaluated in Tables I and II. The best two values for each measurement are underlined.

Table I describes the device efficiency with respect to the use of its actuator. First, $< \tau_m >$, the average torque required to provide a 5 N force at the end effector is given. Then, the maximum torque variation $\Delta\tau_{max}$ over the workspace is calculated and normalized. Finally, the dimensions of the system are given.

Mechanism	$< \tau_m >$	$\frac{\Delta\tau_{max}}{<\tau_m>}$	Dimensions
Hoeken	$\underline{164}$ mN · m	$\underline{0.012}$	115×120 mm
Roberts	397 mN · m	0.271	$\underline{80 \times 45}$ mm
Chebychev	417 mN · m	0.190	$\underline{105 \times 125}$ mm
Chebychev V	$\underline{116}$ mN · m	$\underline{0.015}$	135×105 mm

TABLE I

TORQUES AND BULK CHARACTERISTICS

Table II is related to the characterization of the end effector motion. Let x and y denote the coordinates of the end effector in a frame placed at the origin of the end effector motion, and oriented towards the end effector final point (see figure in table II). Then $(\Delta y)_{max}$ denotes the maximum deviation of the tip from the ideal straight path ($y = 0$) and $(\frac{\Delta y}{\Delta x})_{max}$ indicates locally when the path is not fully rectilinear, which could be sensed by the operator. Finally, the linearity of the relation between the input angle φ_1 and the output position x is quantified by an index, called linearity, as defined by the figure in table II. The value corresponds to the worst case. As the system model is perfectly known, note that a small lack of linearity of $x(\varphi_1)$ is not determining however.

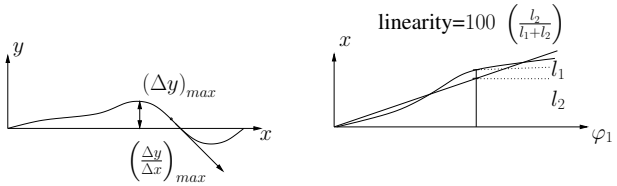

Mechanism	$(\Delta y)_{max}$	$\left(\frac{\Delta y}{\Delta x}\right)_{max}$	Linearity $x(\varphi_1)$
Hoeken	$\underline{0.2}$ mm	$\underline{0.014}$	$\underline{99.0\%}$
Roberts	0.3 mm	0.050	81.9%
Chebychev	$\underline{0.1}$ mm	$\underline{0.015}$	87.5%
Chebychev V	2.4 mm	0.169	$\underline{99.1\%}$

TABLE II

GEOMETRY CHARACTERISTICS

C. Mechanism selection

The two most interesting mechanisms are the Hoeken's mechanism and the Chebychev V one, principally because of the good adequation between their workspace and the reachable tip force. For the same translation range, Roberts mechanism is more compact. However, it is not sufficient to increase its dimensions up to those of the Hoeken's linkage to obtain equivalent tip force. The main drawback of Chebychev V mechanism is the poor linearity of its path whose curvature could be detectable when manipulating the device. As a result, we selected the Hoeken's mechanism to build a prototype.

Its characteristics, summarized in the previous tables, are illustrated more in detail by figure 3.

The variations of the torque that is necessary to obtain a given end effector force are very limited (less than 2 mN · m, for a mean value of 164 mN · m). This confirms that the actuator will be used in an optimal way over the workspace. One can also notice the very good linearity of the end effector position x with respect to the input angle φ_1.

III. PROTOTYPE

A. Hardware

Provided a convenient design of the revolute joints, the different straight line mechanisms can be obtained by fabricating the adequate set of bars. This versatility can be interesting for educational purpose. From now on, we only consider the Hoeken's mechanism that has been fabricated and which is presented in Fig. 4.

The actuator is a DC brushed motor Maxon RE-35 (90 W), with an analog drive that allows to impose precisely the

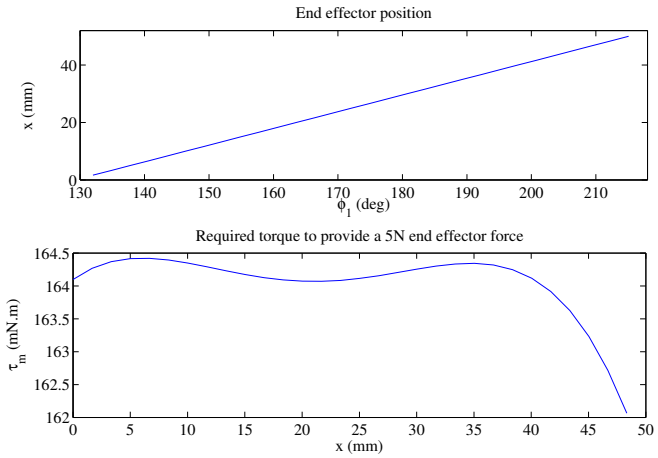

Fig. 3. Hoeken's mechanism characteristics. Top:input/output characteristics linearity; bottom:required torque for a 5 N end effector force (zoom).

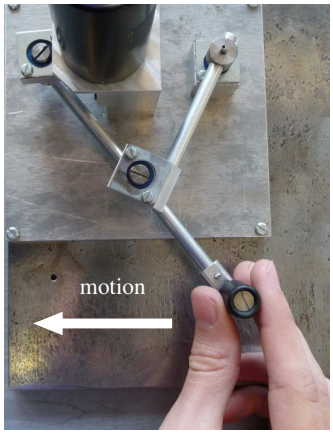

Fig. 4. Fabricated prototype.

motor torque. A continuous force of 3.3 N can be obtained, and then, forces up to 5 N can easily be rendered with an appropriate temperature estimation. A general purpose 2000 counts/rev optical encoder is used. Considering that the motor angular range is limited because of direct drive actuation, a more precise encoder could however be chosen to improve the estimates of velocity and acceleration, and also to improve the possible impedance range. The system control is implemented in a PC equipped with DAC/ADC cards and counter interfaces. It is based on the real-time Linux operating system Xenomai. The frequency rate of the interface sensing and control is 1 kHz, but it can work up to 7 kHz. The control software is generic, open-source, and can be used either for simulation or teleoperation.

B. Prototype characterization

1) Bandwidth: To study the bandwidth of the mechanism an ATI Nano 17 force sensor has been set up on the end effector. Then, the end effector was tied to the ground. The experimental setup is pictured in Fig. 5. A complex sinusoidal torque with variable frequency was applied to the motor. The resulting gain diagram is given in Fig. 5 From

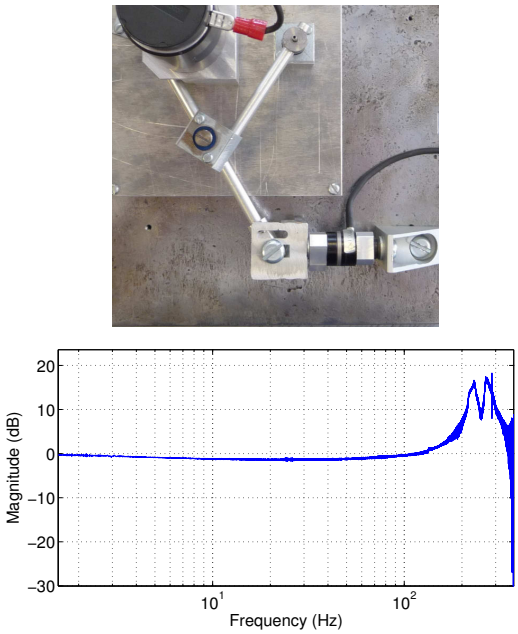

Fig. 5. End effector (equipped with a Nano 17 force sensor) tied to ground. Plot of the system bandwidth.

the experiments, we measure a 150 Hz bandwidth (3 dB cutoff frequency) with a 250 Hz resonance frequency (16 dB peak). This resonance is probably due to some flexibility in the revolute joints. Potentially, it can partly be linked to the way the system is tied to the ground.

2) Modeling and identification methods: The kinetic energy of the mechanism is:

$$T = \frac{1}{2} D \dot{\varphi}_1^2 \tag{13}$$

with D the equivalent moment of inertia of the system at the motor shaft. After calculation, it can be stated that:

$$D = H_{11} + 2H_{12}\cos(\varphi_1 - \varphi_2)\,\alpha_1 + H_{22}\alpha_1^2 + H_{33}\alpha_2 \tag{14}$$

with:

$$\alpha_1 = \frac{l_1 \sin(\varphi_3 - \varphi_1)}{l_2 \sin(\varphi_2 - \varphi_3)},\ \alpha_2 = \left(\frac{l_1 \sin(\varphi_2 - \varphi_1)}{l_3 \sin(\varphi_2 - \varphi_3)}\right)^2 \tag{15}$$

and:

$$H_{11} = m_1 {l_{G1}}^2 + m_2 {l_1}^2 + J_m + J_1 \tag{16}$$

$$H_{22} = m_2 {l_{G2}}^2 + J_2 \tag{17}$$

$$H_{33} = m_3 {l_{G3}}^2 + J_3 \tag{18}$$

$$H_{12} = m_2 l_1 l_{G2} \tag{19}$$

where m_i, l_{Gi} and J_i respectively define the mass, the position of the center of mass and the inertia of the i^{th} link. J_m is the inertia of the motor.

For the Hoeken's mechanism, the end effector translation is along the $-\overrightarrow{x_0}$ direction. So, it comes from equation (12) that:

$$\begin{pmatrix} \dot{x} \\ \dot{y} \end{pmatrix} = \begin{pmatrix} -\dot{x}_e \\ -\dot{y}_e \end{pmatrix} = -J\dot{\varphi}_1 \tag{20}$$

As a result, equation (13) finally writes:

$$T = \frac{1}{2} \begin{pmatrix} \dot{x} \\ \dot{y} \end{pmatrix}^T \mathcal{M} \begin{pmatrix} \dot{x} \\ \dot{y} \end{pmatrix} \tag{21}$$

with:

$$\mathcal{M} = J^{+T} D J^{+} = \begin{pmatrix} M_{11} & M_{12} \\ M_{12} & M_{22} \end{pmatrix} \tag{22}$$

the symmetrical mass matrix of the system (expressed in the operational space). The evolution of $\mathcal{M}$ coefficients are represented in Fig. 6, using the following parameters obtained from the CAD software (in kg.m^2): $H_{11} = 2.97\ 10^{-5}$, $H_{22} = 1.17\ 10^{-4}$, $H_{33} = 7.09\ 10^{-5}$ and $H_{12} = 3.22\ 10^{-5}$. As expected, the mass M_{11} along the x coordinate is

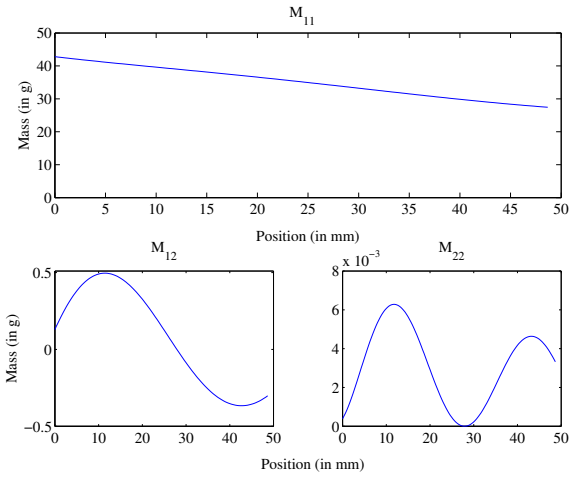

Fig. 6. Evolution of mass matrix coefficients along the workspace.

predominant and fluctuates between 42.8 g and 27.5 g. M_{12} fluctuates between 0.5 g and -0.4 g and M_{22} is very small, so that the dynamics effects in the y direction are negligible.

From this observation, we can simplify the writing of the dynamical model in the operational space by considering only the projection along the x direction, that is:

$$F_m^x = M_{11}\ddot{x} + F_v\dot{x} + F_s \text{ sign } \dot{x} + c_x \tag{23}$$

where F_m^x is the force applied by the motor to the mechanism along x, M_{11} is the apparent mass, $\dot{x}$ and $\ddot{x}$ are respectively the velocity and the acceleration of the end effector, F_v is the viscous friction coefficient, F_s the Coulomb friction coefficient and c_x an offset. All these parameters are interesting from a haptic point of view and can therefore be identified using a proper method.

As the system is torque controlled, an open-loop identification method cannot be implemented easily. Then, a close-loop identification has been used according to Fig. 7 scheme. A joint position control loop is used to move the system, generally with sinusoidal motions. In order to add a persistent excitation, a pseudo-random binary sequence (PRBS) can be superimposed to the control signal. As the joint velocities and the joint accelerations are derived from the joints position, a low-pass 6-th order Butterworth filter is used to reduce the noise.

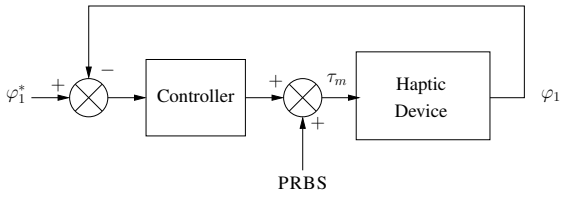

Fig. 7. Closed-loop identification scheme.

Two experimental sets with different inputs have been carried out. The first data set is used to identify the parameters, whereas the second data set is used to validate the estimation accuracy. The result of this procedure is illustrated by the plot of the applied and the estimated forces in Fig. 8. The identified parameters are $M_{11} = 44$ g, $F_v = 1.2\ 10^{-1}\text{N} \cdot \text{s} \cdot \text{m}^{-1}$, $F_s = 7.4\ 10^{-2}$ N and $c_x = -1.8\ 10^{-2}$ N. The apparent mass is then slightly

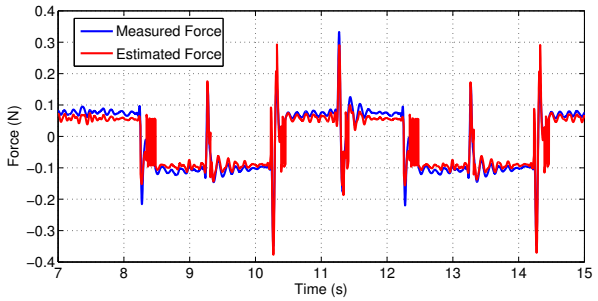

Fig. 8. Validation of the dynamic model identification.

greater than expected from modeling and CAD values.

3) Refinements for Coulomb friction estimation: Coulomb friction can also be identified separately, to refine the previous results. To that purpose, a sinusoidal trajectory was generated while the system was controlled in position with a simple proportional gain and a tachymetric feedback gain. Data were filtered with a 6th-order Butterworth filter designed with a 3 Hz cutoff frequency in order to keep only very slow motion informations. A forward-backward filtering method implemented in the filtfilt function of Matlab was used in order to avoid any phase shift.

In Fig. 9, the plain line represents Coulomb friction force during a sinusoidal motion centered around the middle of the workspace. We can see that the Coulomb friction is small compared to the available maximum force. As the motion is slow, inertia term is negligible. Fig. 10 is used to determine Coulomb friction assuming the following friction model:

$$F_m^x = F_s \text{ sign } \dot{x} + c_x \tag{24}$$

where the identified parameters are: $F_s = 8.3\ 10^{-2}$ N and $c_x = -1.45\ 10^{-2}$ N.

The characteristics obtained with the model and the validation data lead to the plots in Fig. 10.

4) Evaluation of stiffness capability of the interface: In [11], the authors use a passive approach to characterize the global stability of a haptic interface. To derive less

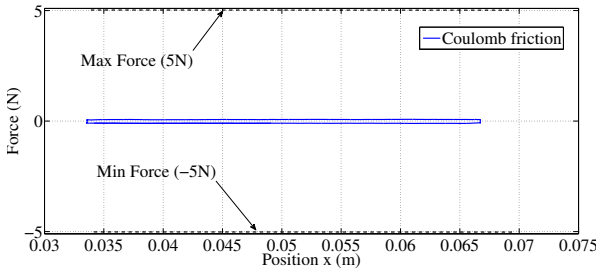

Fig. 9. Force evolution resulting from Coulomb friction.

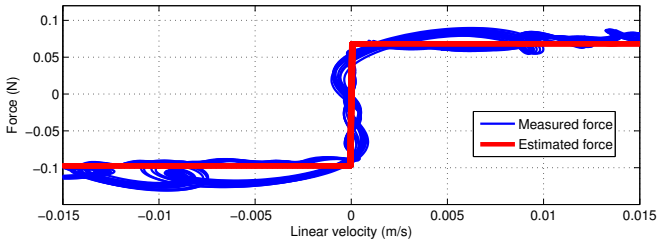

Fig. 10. Coulomb friction identification.

conservative conditions for stability, Diolaiti et al. [12] define local stability for such a system. It results in a larger stiffness range for which the haptic interface remains stable:

$$\frac{2F_v}{T_e} \leq K \leq \frac{2(F_s + F_v \dot{x}_{max})}{\Delta + \dot{x}_{max} T_e} \tag{25}$$

where F_v is the viscous friction coefficient, F_s is the Coulomb friction coefficient, K is the desired stiffnes to render, T_e the sampling period, Δ the elementary translation corresponding to the encoder resolution and $\dot{x}_{max}$ the maximum velocity of the interface before instability. Applying those formulae to our system gives a theoretical stiffness capability of 2500 N/m with $T_e = 0.33$ ms, $\Delta = 5.46\ 10^{-5}$ m and $\dot{x}_{max} = 0.04$ m/s. Nevertheless, experimental results are better and the interface is able to render a stiffness of 15000 N/m before instability occurs. Thus can be explained by the conservative hypothesis expressed in equation (25).

IV. Conclusion

In this paper the use of approximate straight line mechanisms has been proposed to design linear force feedback displays. They have (a 4-bar) parallel architecture which is suitable to improve rigidity, as generally admitted in haptics. At the expense of a relative complexity, these systems do not make use of cables nor linear bearings, thus limiting the drawbacks of these components: friction and flexibilities. These systems, particularly the Hoeken's one, can potentially be used in haptic applications without gears, which may help to obtain interesting displays, both for the purpose of education or research. For instance, we used it at the moment as a master interface in teleoperation experimental testbed to validate the results presented in [13].

A prototype has been built, and both the methods and the results of its characterization have been presented. They demonstrate that the Coulomb friction is not negligible. It is mostly due to the use of a brushed DC motor, which was preferred to prevent from the effects of torque cogging of DC brushless motors. The apparent mass of the system proves to remain below 50 grams, which is certainly enough for such a simple mechanism, and could be reduced by the use of carbon links. It is important to notice that the system can easily be modified to meet other characteristics (translation length and maximum rendering force). Further research is mainly related to the identification of the dynamical model, that could be improved to obtain an even finer description of the system.

Acknowledgment

This work was supported by the Alsace Regional Council and the CNRS.

References

[1] Richard, C., Okamura, A., Cutkosky, M.: Getting a feel for dynamics: Using haptic interface kits for teaching dynamics and controls. In: ASME IMECE 6th Annual Symposium on Haptic Interfaces, Dallas, USA (1997) 15–21

[2] Grow, D., Verner, L., Okamura, A.: Educational haptics. In: AAAI 2007 Spring Symposia - Robots and Robot Venues: Resources for AI Education. (2007)

[3] Rosenberg, L.: Virtual fixtures: Perceptual tools for telerobotic manipulation. In: IEEE Virtual Reality International Symposium. (1993) 76–82

[4] Boldea, I., Nasar, S.: Linear electric actuators and generators. IEEE Transactions on Energy Conversion **14**(3) (1999) 712–717

[5] Etel: Etel – linear motors (2008) `http://www.etel.ch/linear_motors`.

[6] Hayward, V., Astley, O.: Performance measures for haptic interfaces. In: International Symposium in Robotics Research, Springer Verlag (1996) 195–207

[7] Adams, R., Moreyra, M., Hannaford, B.: Excalibur, a three-axis force display. In: ASME Winter Annual Meeting, Symposium on Haptic Interfaces for Virtual Environment and Teleoperator Systems. (1999)

[8] Weir, D.W., Peshkin, M.A., Colgate, J.E., Buttolo, P.: Design and performance of a high fidelity, low mass, linear haptic display. In: IEEE Joint Eurohaptics Conference and Symposium on Haptic Interfaces for Virtual Environment and Teleoperator Systems, Pisa, Italy (2005) 177–182

[9] Barbé, L., Bayle, B., Piccin, O., Gangloff, J., de Mathelin, M.: Design and evaluation of a linear haptic device. In: IEEE International Conference on Robotics and Automation, Roma, Italy (2007) 485–490

[10] Artobolevski, I.: Mechanisms in Modern Engineering Design. Mir Publisher (1975)

[11] Colgate, J., Schenkel, G.: Passivity of a class of sampled-data systems: Application to haptic interfaces. Journal of robotic systems **14**(1) (1997) 37–47

[12] Diolaiti, N., Niemeyer, G., Barbagli, F., Salisbury, J.: Stability of haptic rendering: Discretization, quantization, time delay, and coulomb effects. IEEE Transactions on Robotics **22**(2) (april 2006) 256 –268

[13] Joinié-Maurin, M., Bayle, B., Barbé, L., Gangloff, J.: Force feedback teleoperation with physiological motion compensation. In: 9th International IFAC Symposium on Robot Control, Gifu, Japan (2009)